24th INTERNATIONAL CONGRESS ON SOUND AND VIBRATION
23–27 July 2017, London

EFFECTS OF THE SYSTEM IMPERFECTIONS ON THE ISOLATION PERFORMANCE OF A QUASI-ZERO-STIFFNESS ISOLATOR

Meng Lingshuai, Ren Xudong, Sun Jinggong, Niu Fu, and Xu Xinxi

Institute of Medical Equipment, Academy of Military Medical Sciences, 300161 Tianjin, China
email: mengls1989@sina.com

In view of the low frequency isolation performance and dimensional limit for the isolator used in the vehicle precision instruments, a novel quasi-zero-stiffness (QZS) isolator is designed by combining parallelly a negative stiffness disk spring with a linear positive stiffness spring. The static characteristics of the disk spring and QZS isolator are studied. The combination of the configurative parameters is derived to achieve zero stiffness at the equilibrium position. The nonlinear dynamic equations are established for the system under harmonic force and displacement excitations. By using the averaging method, the effects of system imperfections on the force transmissibility and the displacement transmissibility are studied. The stability is analysed by applying Mathieu equation discriminant method. Compared with the equivalent linear system, the system is superior in the low frequency and ultra-low frequency vibration isolation. The results can offer theoretical guidance in the design and application of the QZS isolator.
Keywords: QZS isolator, system imperfection, transmissibility, averaging method

1. Introduction

Owing to the better vibration isolation performance than linear isolators in low frequency region, passive nonlinear vibration isolators have drawn much attention in the scientific and industrial fields. Ibrahim introduced the recent advances in passive nonlinear vibration isolators and described their main nonlinear characteristics in detail [1]. A comprehensive review on passive nonlinear vibration isolators was presented by Alabuzhev et al. [2], in which a large number of prototypes utilizing negative stiffness structure have resulted in low frequency isolation and excellent support capacity. Carrella et al. proposed a high-static-low-dynamic-stiffness isolator by connecting a vertical coil spring and two oblique coil springs [3-5]. Le and Ahn proposed a nonlinear isolator using a horizontal spring in series with a bar as negative stiffness structure [6, 7]. Liu et al. carried out a research on Euler buckled beam to work as negative stiffness corrector to realize a quasi-zero stiffness isolator [8-10]. Xu et al. proposed a nonlinear magnetic vibration isolator with quasi-zero characteristic [11]. Lan et al. designed a vibration isolator capable of isolating a wide range of loads in low frequency region [12]. Zhou et al. investigated a quasi-zero stiffness isolator with cam-roller mechanism [13].

In this paper we propose a new QZS isolator by combining a disk spring with a vertical linear spring. Compared with other negative stiffness elements, taking a disk spring as negative stiffness element can offer greater support capacity because the disk spring can bear great load with small deflection and supply a certain restoring force at the flatten state. Therefore, the new QZS isolator is suitable for being used in the occasion with space limitation for isolators. Meanwhile, its axial nonlinear restoring force enables the isolator to achieve the QZS property at the static equilibrium position.

2. Static characteristics

2.1 Disk spring

A modal schematic of a disk spring is shown in Fig. 1. The disk spring supported at points A, B, C and D has an axial deflection x under the applied force P. The relationship can be expressed by

$$P=\frac{2\pi Ex}{\left(e_1-e_2\right)^2\left(1-\mu^2\right)}\left\{\left[\frac{1}{2}\left(e_1^2-e_2^2\right)-\frac{\left(e_1-e_2\right)^2}{\ln\frac{e_1}{e_2}}\right]\left(\frac{h}{a-b}-\frac{x}{e_1-e_2}\right)\left(\frac{h}{a-b}-\frac{x}{2\left(e_1-e_2\right)}\right)t_c+\frac{t_c^3}{12}\ln\frac{e_1}{e_2}\right\}, \quad (1)$$

where a is the external radius, b is the internal radius, h is the free height, t_c is the thickness, E is the Young's modulus, μ is the Poisson's ratio, e_1 and e_2 are the distances of the supporting points to the center line. Eq. (1) can be simplified as

$$P=\frac{Ex}{e_1^2\left(1-\mu^2\right)}\left[\left(\bar{h}-x\right)\left(\bar{h}-\frac{x}{2}\right)\frac{t_c}{M}+\frac{t_c^3}{N}\right], \quad (2)$$

where $\bar{h}=h/\Lambda$ is the equivalent height and $C=e_1/e_2$ is ratio of supporting points. The parameters Λ, M and N are defined as

$$\Lambda=(a-b)/(e_1-e_2),\ \frac{1}{M}=\pi\left(\frac{C+1}{C-1}-\frac{2}{\ln C}\right)\left(\frac{C}{C-1}\right)^2,\ \frac{1}{N}=\frac{\pi}{6}\left(\frac{C}{C-1}\right)^2\ln C. \quad (3a\text{-}c)$$

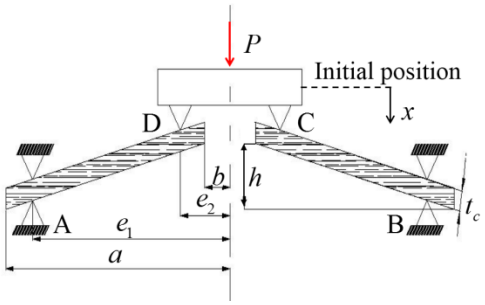

Figure 1: Schematic representation of the disk spring.

With the disk spring moving down from the initial position $x=0$, it starts to provide a restoring force F_d. When the disk spring is in a horizontal line which means $x=x_e=\bar{h}$, the restoring force $F_d>0$. Note that the force-displacement curve is symmetric about the point $\left(x_e,F_{de}\right)$ as x changes during the range $\left[0,2\bar{h}\right]$. Setting this point as the origin of a new vertical displacement coordinate u and defining the following non-dimensional parameters:

$$\hat{F}_d=\frac{F_d e_1^2\left(1-\mu^2\right)M}{Et_c^4},\ \hat{u}=\frac{u}{t_c},\ \alpha=\frac{\bar{h}}{t_c},\ \Gamma=\frac{M}{N}. \quad (4a\text{-}d)$$

The non-dimensional restoring force can be expressed as

$$\hat{F}_d=\frac{1}{2}\hat{u}^3+\left(\Gamma-\frac{1}{2}\alpha^2\right)\hat{u}+\alpha\Gamma, \quad (5)$$

where $\hat{u}=\hat{x}-\alpha$ and α is the ration between equivalent height and thickness.

By differentiating Eq. (5) with respect to the non-dimensional displacement $\hat{u}$, the non-dimensional stiffness of the disk spring $\hat{k}$ can be derived as

$$\hat{k}_d=\frac{3}{2}\hat{u}^2+\Gamma-\frac{1}{2}\alpha^2. \quad (6)$$

Considering the parameters $C = e_1/e_2 > 1$ and $\Gamma > 0$, it can be seen that the non-dimensional stiffness is symmetric about $\hat{u} = \hat{u}_e = 0$ and gets the minimum value $\hat{k}_{d\min} = \Gamma - \alpha^2/2$ at this position. To achieve the continuous negative stiffness region, the parameters should meet the condition $\alpha > \sqrt{2\Gamma}$. And the continuous negative stiffness region can be derived as

$$\hat{u} \in \left(-\sqrt{(\alpha^2 - 2\Gamma)/3}, \sqrt{(\alpha^2 - 2\Gamma)/3}\right). \tag{7}$$

Note that the minimum value $\hat{k}_{d\min}$ and the negative stiffness region are related with the parameters α and C. The disk spring owns smaller $\hat{k}_{d\min}$ and larger negative stiffness region with increasing α and decreasing C.

2.2 The QZS isolator

The schematic of the proposed QZS isolator is shown in Fig. 2. A disk spring acting as the negative stiffness structure and a vertical linear spring k_l are connected to the isolated mass m. Ignoring the isolated mass, the restoring force of the QZS isolator can be expressed by

$$F_r = F_l + F_d = k_v x + \frac{Ex}{e_1^2\left(1-\mu^2\right)}\left[\left(\bar{h} - x\right)\left(\bar{h} - \frac{x}{2}\right)\frac{t_c}{M} + \frac{t_c^3}{N}\right], \tag{8}$$

where F_l and F_d are the restoring forces of the linear spring and the disk spring at axial direction separately.

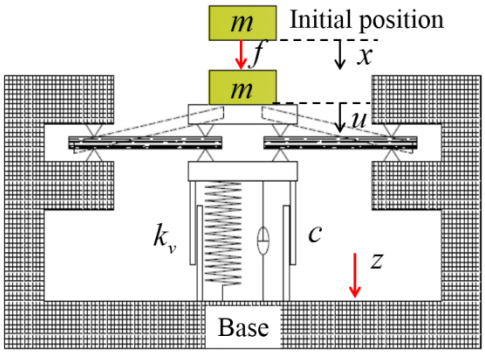

Figure 2: Schematic representation of the QZS isolator.

The non-dimensional restoring force of the QZS isolator can be derived as

$$\hat{F}_r = \hat{u} + \alpha + \lambda\left[\frac{1}{2}\hat{u}^3 + \left(\Gamma - \frac{1}{2}\alpha^2\right)\hat{u} + \alpha\Gamma\right], \tag{9}$$

where $\hat{F}_r = \hat{F}_r/(k_v t_c)$ and $\lambda = Et_c^3/\left[k_v e_1^2\left(1-\mu^2\right)M\right]$ is defined as the stiffness ratio between the disk spring and the linear spring.

By differentiating Eq. (9) with respect to the non-dimensional displacement $\hat{u}$, the non-dimensional stiffness of the QZS isolator can be derived as

$$\hat{k} = 1 + \lambda\left(\frac{3}{2}\hat{u}^2 - \frac{1}{2}\alpha^2 + \Gamma\right), \tag{10}$$

where $\hat{k} = k/k_v$.

When the disk spring is horizontal, i.e. $\hat{u} = \hat{u}_e = 0$, the non-dimensional stiffness of the isolator is symmetric about the position and has the minimum value. In operation, the isolator is prospected to own zero stiffness and reach static equilibrium at this position with an appropriate mass. By setting Eq. (10) to zero at $\hat{u} = \hat{u}_e = 0$, the desired stiffness ratio can be derived by

$$\lambda_{QZS} = \frac{2}{\alpha^2 - 2\Gamma}. \tag{11}$$

Fig. 3 shows the non-dimensional stiffness-displacement curves with different α and C. It can be seen that the QZS isolator possesses smaller stiffness in the neighborhood of the static equilibrium position and larger displacements of smaller stiffness with increasing α and decreasing C.

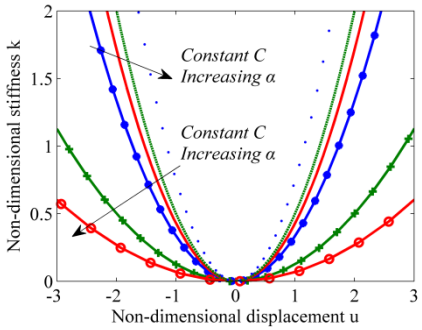

Figure 3: Non-dimensional stiffness characteristics of the QZS isolator.

3. Dynamic characteristics

3.1 Manuscript Title Dynamic modeling and solution

It is prospected that QZS isolator loaded with an appropriate mass can keep balance at the static equilibrium position $\hat{u} = \hat{u}_e = 0$. And the static equilibrium position is also a zero stiffness position. Based on Eqs. (9) and (11), the quantity of the mass should satisfy the condition

$$mg = \frac{\alpha^3}{\alpha^2 - 2\Gamma} k_v t_c. \tag{12}$$

According to Fig. 2, two types of excitations are considered: one is the harmonic force excitation $f = F\cos(\omega t)$ on the mass; the other one is the harmonic displacement excitation $z = Z\cos(\omega t)$ on the base. By using the Newton's second law of motion, one can achieve the dynamic equations separately for the two types of excitations given above

$$m\ddot{u} + c\dot{u} + F_{r1} - mg = F\cos(\omega t),\ m\ddot{y} + c\dot{y} + F_{r2} - mg = m\omega^2 Z\cos(\omega t), \tag{13a, b}$$

where $y = u - z$ is the relative displacement between the base and the mass, F_{r1} and F_{r2} are the restoring forces under the two types of excitations. Combining Eq. (12) and introducing the non-dimensional parameters as follows:

$$\tau = \omega_n t,\ \Omega = \frac{\omega}{\omega_n},\ \omega_n = \sqrt{\frac{k_v}{m}},\ \hat{y} = \frac{y}{t_c},\ \xi = \frac{c}{2m\omega_n},\ \hat{F} = \frac{F}{k_v t_c},\ \hat{Z} = \frac{Z}{t_c}. \tag{14a-g}$$

Eq. (13) can be rewritten as the non-dimensional form:

$$\hat{u}'' + 2\xi\hat{u}' + \chi\hat{u}^3 = \hat{F}\cos(\Omega\tau),\ \hat{y}'' + 2\xi\hat{y}' + \chi\hat{y}^3 = \Omega^2\hat{Z}\cos(\Omega\tau), \tag{15a, b}$$

where $\chi = 1/(\alpha^2 - 2\Gamma)$ and $(\square)' = d(\square)/d\tau$.

Eq. (15) can be expressed by a uniform dynamic equation for simplicity:

$$\hat{v}'' + 2\xi\hat{v}' + \chi\hat{v}^3 = \gamma\rho\cos(\Omega\tau), \tag{16}$$

where ρ is the amplitude of the harmonic excitations. For the force excitation: $\gamma = 1$, $\rho = \hat{F}$; For the displacement excitation, $\gamma = \Omega^2$, $\rho = \hat{Z}$.

By removing the disk spring, the equivalent linear system (ELS) to the QZS isolator can be obtained. The dynamic equation of the ELS is

$$\hat{v}'' + 2\xi\hat{v}' + \hat{v} = \gamma\rho\cos(\Omega\tau). \tag{17}$$

Then the amplitude of the steady-state response for ELS can be derived as

$$A=\frac{\gamma\rho}{\sqrt{\left(1-\Omega^2\right)^2+\left(2\xi\Omega\right)^2}}. \tag{18}$$

As shown in Eq. (16), it can be seen that the QZS system is a Duffing oscillator under symmetric excitation. The average method is employed to get the approximate steady-state solution. The steady-state solution of the nonlinear system can be assumed to be

$$\hat{v}=A_1\cos\left(\Omega\tau+\varphi\right),\ \hat{v}'=-\Omega A_1\sin\left(\Omega\tau+\varphi\right), \tag{19a, b}$$

where the amplitude of the harmonic term A and the phase φ are related with the time τ.

Then the following equations can be derived as

$$A'=-\frac{1}{\Omega}\Pi\sin\left(\Omega\tau+\varphi\right),\ \varphi'=-\frac{1}{A_1\Omega}\Pi\cos\left(\Omega\tau+\varphi\right). \tag{20a, b}$$

Letting $A'=\varphi'=0$, which physically implies that the time-averaged rates of change of amplitude and phase angle vanish, one can get

$$-\frac{\gamma\rho\sin\left(\varphi\right)}{2\Omega}-\xi A_1=0,\ -\frac{\gamma\rho\cos\left(\varphi\right)}{2\Omega A_1}-\frac{\Omega}{2}+\frac{3\chi A_1^2}{8\Omega}=0. \tag{21a, b}$$

Combining Eqs. (21a, b), one can get the implicit amplitude frequency equation of the QZS system

$$\left(\frac{3}{4}\chi A^3-\Omega^2 A\right)^2+4\xi^2\Omega^2A^2=\gamma^2\rho^2. \tag{22}$$

3.2 Transmissibility

The key indexes to evaluate the performance of an isolator are the force transmissibility for the force excitation and the absolute displacement transmissibility for the displacement excitation.

The force transmissibility is defined as the ratio between the amplitude of the non-dimensional dynamic force transmitted to the base and that of the non-dimensional excitation force. It can be expressed by

$$T_f=\frac{\hat{F}_t}{\rho}, \tag{23}$$

where $\hat{F}_t=\sqrt{\hat{F}_{td}^2+\hat{F}_{te}^2}=\sqrt{\left(2\xi\Omega A\right)^2+\left(\frac{3}{4}\chi A^3\right)^2}$.

The absolute displacement transmissibility is defined as the ratio between the amplitude of the non-dimensional absolute displacement of the mass and non-dimensional excitation displacement. It is given by

$$T_z=\frac{\left|\hat{u}\right|}{\left|\hat{z}\right|}=\frac{\sqrt{A^2+\rho^2+2A\rho\cos\left(\varphi\right)}}{\rho}, \tag{24}$$

where $\cos\left(\varphi\right)$ is defined by Eq. (21b).

The force and absolute displacement transmissibilities of the ELS have the same expression as [3]

$$T_l=\sqrt{\frac{1+\left(2\xi\Omega\right)^2}{\left(1-\Omega^2\right)^2+\left(2\xi\Omega\right)^2}}. \tag{25}$$

4. Effects of the system imperfection on the isolation performance

Based on the above analysis, the transmissibility curves with different system imperfections are plotted in Figs. 4-6. Fig. 4 shows the effects of the excitation amplitude on the isolation performance. It can be seen that the QZS system has a lower starting frequency and a larger frequency

range of isolation effects than the ELS. Different from that of the ELS independent of the excitation amplitude, the peak amplitude of the transmissibilities and the corresponding resonance frequency of the QZS system decreases as the excitation amplitude decreases, which means that the QZS system has superior isolation performance in low frequency range than the ELS.

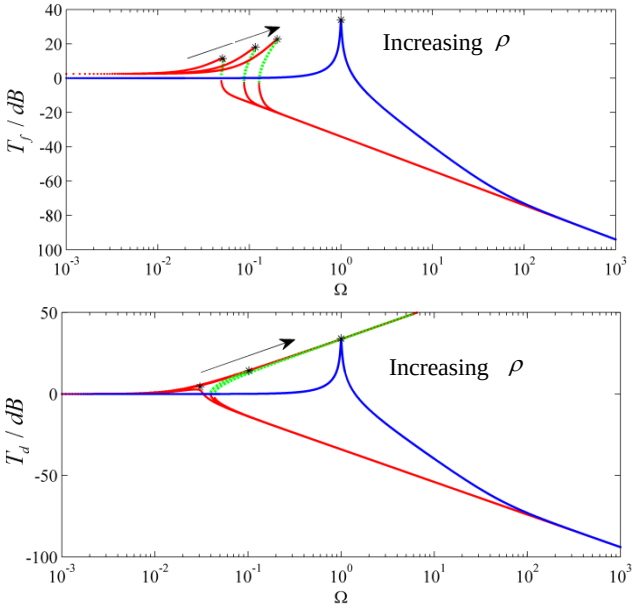

Figure 4: Effects of the excitation amplitude on the isolation performance. 'red line' the QZS system; 'blue line' the ELS; 'green dotted line' unstable solutions; '$*$'peak amplitude of transmissibility.

Fig. 5 shows the effects of the damping ratio on the isolation performance. As the damping ratio increases, the peak amplitudes of the transmissibilities decrease and the transmissibilities in higher frequency range increase for the two systems. Note that the QZS system can get smaller resonance frequency and unstable region with increasing damping ratio. If the damping ratio is large enough, the peak amplitudes of the transmissibilities and unstable regions of the QZS system will not occur.

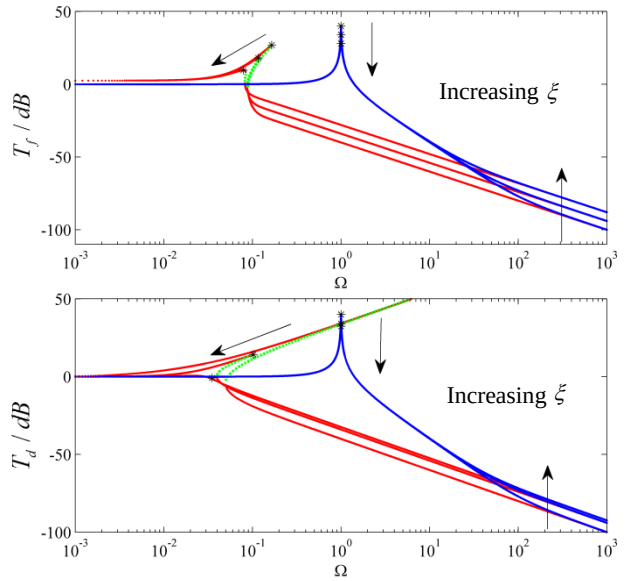

Figure 5: Effects of the damping ratio on the isolation performance. 'red line' the QZS system; 'blue line' the ELS; 'green dotted line' unstable solutions; '$*$'peak amplitude of transmissibility.

Fig. 6 shows the effects of the nonlinear term χ on the isolation performance. It can be found that the effects of the nonlinear term χ are similar with that of the excitation amplitude. And the effects are obvious in the neighborhood of the resonance frequency. The starting frequency of isola-

tion effects, the peak amplitudes of the transmissibilities and the unstable region get smaller as he nonlinear term χ decreases, which means that a smaller nonlinear term χ leads to a better isolation performance in low frequency range.

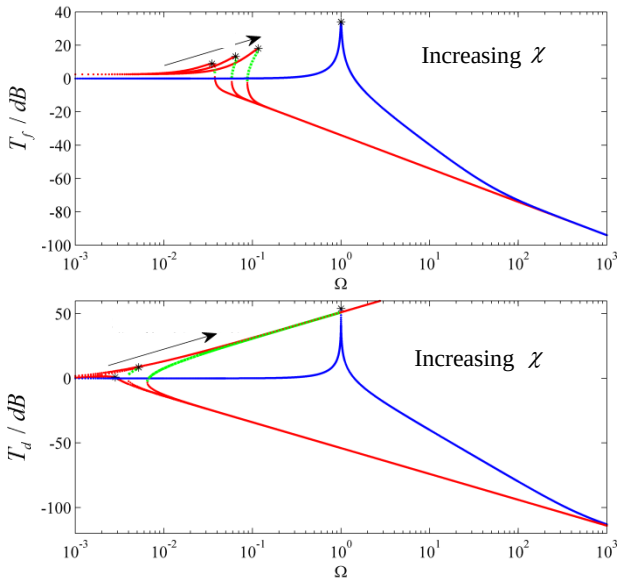

Figure 6: Effects of the nonlinear term χ on the isolation performance. 'red line' the QZS system; 'blue line' the ELS; 'green dotted line' unstable solutions; '$*$'peak amplitude of transmissibility.

5. Stability analysis

On account of the appearance of multiple values for the steady-state solution, the Mathieu equation discriminant method is used to study the stability of the steady-state solution. Superposing a small non-dimensional perturbation $\hat{\varepsilon}(\tau)$ to the steady-state solution, one can get

$$\hat{v} = A\cos(\Omega\tau + \varphi) + \hat{\varepsilon}(\tau). \tag{26}$$

By substituting Eq. (26) into Eq. (16), the equation for the perturbation can be derived as

$$\varepsilon''(\tau) + 2\xi\varepsilon'(\tau) + \frac{3}{2}\chi A_1^2\left[1+\cos 2(\Omega\tau+\varphi)\right]\varepsilon(\tau) = 0. \tag{27}$$

Supposing that

$$\varepsilon = E_1\cos(\vartheta) + E_2\sin(\vartheta), \tag{28}$$

and substituting Eq. (28) into Eq. (27), one can achieve that

$$\begin{aligned}&\left(-\Omega^2 E_1 + \frac{9}{4}\chi A_1^2 E_1 + 2\xi\Omega E_2\right)\cos(\vartheta) + \left(-\Omega^2 E_2 + \frac{3}{4}\chi A_1^2 E_2 - 2\xi\Omega E_1\right)\sin(\vartheta)\\ &+\frac{3}{4}\chi A_1^2 E_1\cos(3\vartheta) + \frac{3}{4}\chi A_1^2 E_2\sin(3\vartheta) = 0\end{aligned}. \tag{29}$$

Neglecting the high order harmonic term and setting the coefficients of $\cos(\vartheta)$ and $\sin(\vartheta)$ to zero, one can get the following equations

$$\begin{cases}\left(\frac{9}{4}\chi A_1^2 - \Omega^2\right)E_1 + 2\xi\Omega E_2 = 0\\ -2\xi\Omega E_1 + \left(\frac{3}{4}\chi A_1^2 - \Omega^2\right)E_2 = 0\end{cases}. \tag{30}$$

When the determinant of the matrix in Eq. (30) vanishes, the boundary between the stable and unstable regions can be achieved as

$$\Delta = \Omega^4 + \left(4\xi - 3\chi A_1^2\right)\Omega^2 + \frac{27}{16}\chi^2 A_1^4 = 0. \tag{31}$$

The unstable region occurs when $\Delta < 0$, which is plotted by green dotted line in Figs. 4-6.

6. Conclusion

In this paper, we introduce the theoretical design and characteristics analysis of a novel QZS isolator. The QZS isolator is developed by adding a disk spring with negative stiffness to a vertical linear spring with positive stiffness. The vibration isolation performances of the QZS system and its ELS are studied under different system imperfections, such as excitation amplitude, damping ratio, nonlinear term et al. By decreasing the excitation amplitude and the nonlinear term, and increasing the damping ratio appropriately, the QZS system can achieve a lower starting frequency of isolation effects and smaller peak amplitudes of the transmissibilities. The conclusion can be drawn that the QZS system can exhibit superior isolation performance in low frequency range compared with its ELS.

REFERENCES

1 Ibrahim, R. A., Recent advances in nonlinear passive vibration isolators, Journal of Sound and Vibration, 314, 71-452, (2008).

2 Alabuzhev, P., Gritchin, A., Kim, L., Migirenko, G., Chon, V. and Stepanov P. Vibration Protecting and Measuring Systems with Quasi-Zero Stiffness, Hemisphere, New York (1989).

3 Carrella, A., Brennan, M. J. and Waters T. P. Static analysis of a passive vibration isolator with quasi-zero-stiffness characteristic, Journal of Sound and Vibration, 301, 678-689, (2007).

4 Carrella, A., Brennan, M. J., Waters, T. P. and Shin K. On the design of a high-static-low- dy-namic stiffness isolator using linear mechanical springs and magnets, Journal of Sound and Vibration, 315, 712-720, (2008).

5 Carrella A., Passive vibration isolators with high-static-low-dynamic-stiffness, Ph.D. Thesis, ISVR, University of Southampton, (2008).

6 Le, T. D. and Ahn, K. K. A vibration isolation system in low frequency excitation region using negative stiffness structure for vehicle seat, Journal of Sound and Vibration, 330, 631-6335, (2011).

7 Le, T. D. and Ahn, K. K. Experimental investigation of a vibration isolation system using negative stiffness structure, International Journal of Mechanical Sciences, 70, 99-112, (2013).

8 Liu, X. T., Huang, X. C., and Hua H. X. On the characteristics of a quasi-zero stiffness isolator using Euler buckled beam as negative stiffness corrector, Journal of Sound and Vibration, 332, 3359-3376, (2013).

9 Huang, X. C., Liu, X. T., Sun, J. Y., Zhang, Z. Y., Hua, H. X. and Hua, H. X. Vibration isolation characteristics of a nonlinear isolator using Euler buckled beam as negative stiffness corrector: A theoretical and experimental study, Journal of Sound and Vibration, 333, 1132-1148, (2014).

10 Huang, X. C., Liu, X. T., and Hua, H. X. Effects of stiffness and load imperfection on the isolation performance of a high-static-low-dynamic-stiffness non-linear isolator under base displacement excitation, International Journal of Non-Linear Mechanics, 65, 32-43, (2014).

11 Xu, D. L., Yu, Q. P., Zhou, J. X., and Bishop, S. R. Theoretical and experimental analyses of a nonlinear magnetic vibration isolator with quasi-zero-stiffness characteristic, Journal of Sound and Vibration, 332, 3377-3389, (2013).

12 Lan, C. C., Yang, S. A. and Wu, Y. S. Design and experiment of a compact quasi-zero-stiffness isolator capable of a wide range of loads, Journal of Sound and Vibration, 333, 4843-4858, (2014).

13 Zhou, J. X., Wang, X. L., Xu, D. L. and Zhang, J. Experimental study on vibration isolation characteristics of the quasi-zero stiffness with cam-roller mechanism, Journal of Vibration Engineering, 28, 449-455, (2015). (in chinese)